MALAYSIAN JOURNAL OF SCIENCE
MJS
ISSN 1394-3065

Regular Issue

Malaysian Journal of Science 42 (3): 13-19 (Oct 2023) https://mjs.um.edu.my

NUMERICAL SIMULATION OF ENHANCED OPTICAL FREE SPECTRAL RANGE THROUGH INTEGRATED FANO-MICRORING CONFIGURATION

Mohammad Amirul Hairol Aman[1a,b], Ahmad Fakhrurrazi Ahmad Noorden[2a,b]*, Faris Azim Ahmad Fajri[3a,b], Muhammad Zamzuri Abdul Kadir[4a,b], Wan Hazman Danial[5c], Suzairi Daud[6d]

Abstract: A numerical analysis of the integrated Fano-microring (IFM) racetrack resonator spectrum was performed to investigate the enhancement of the optical system's free spectral range (FSR). The FSR is an important optical property which can contribute to the high sensitivity of optical devices. The IFM refers to the combination of Fano resonance produced in the output spectrum through the interaction of Fabry–Perot resonance and circulation resonance. This work focuses on the study of inducing Fano resonance in the microring resonator to optimize the FSR of the system. The results show that the integration of two resonances can produce a Vernier output spectrum, which significantly enhanced the FSR of the system without any need for additional ring waveguides. This work also compared the IFM resonance with the conventional microring resonance. In this simulation, the optimized FSR obtained by the IFM configuration was 266.55 nm, which is five times higher than the conventional microring configuration.

Keywords: *Fano resonance, microring, free spectral range, fabry-perot resonance, numerical simulation*

1. Introduction

Optical microring resonators have been applied in various devices and fields, such as sensor technology, including pressure sensors (Seyfari et al., 2020), thermal sensors (Zhu & Lou, 2020), gas sensors (Koushik & Malathi, 2020), and chemical sensors (Bavili et al., 2020). Microring has also been applied as a modulator (Moradi et al., 2021) and an optical switch (Bharti & Rakshit, 2021; Singh et al., 2021) due to its compact size (Biswas et al., 2021), high compatibility (Bogaerts et al., 2012), low cost (Kim et al., 2013), and utilization of evanescence field that makes it immune towards electromagnetic disturbances (Bogaerts et al., 2012). Consequently, performance is essential in the advancement of this technology.

Authors information:
[a]Centre for Advanced Optoelectronics Research (CAPTOR), Kulliyyah of Science, International Islamic University Malaysia, 25200 Kuantan, Pahang, MALAYSIA. E-mail: amirul.hairol@live.iium.edu.my[1], fakhrurrazi@iium.edu.my[2], azim10miza@gmail.com[3], zamzurikadir@iium.edu.my[4]
[b]IIUM Photonics and Quantum Centre (IPQC), Kulliyyah of Science, International Islamic University Malaysia, 25200, Kuantan, Pahang, MALAYSIA. E-mail: amirul.hairol@live.iium.edu.my[1], fakhrurrazi@iium.edu.my[2], azim10miza@gmail.com[3], zamzurikadir@iium.edu.my[4]
[c]Department of Chemistry, Kulliyyah of Science, International Islamic University Malaysia, 25200, Kuantan, Pahang, MALAYSIA. E-mail: whazman@iium.edu.my[5]
[d]Laser Center, Ibnu Sina Institute for Scientific & Industrial Research, Universiti Teknologi MALAYSIA, 81310, Johor Bahru, Johor, Malaysia. E-mail: suzairidaud@utm.my[6]
*Corresponding Author: fakhrurrazi@iium.edu.my

Limit of detection (LOD) is one of the indicators to evaluate the performance of microring configuration in sensing application. LOD can be described as the minimum detectable change (Guider et al., 2015), which is directly related to free spectral range (FSR) (Vollmer & Schwefel, 2014). FSR can be interpreted as the distance between two adjacent peaks (Bogaerts et al., 2012). The relationship of LOD and FSR is inversely proportional, where higher FSR will offer smaller detectable scale (Chao & Guo, 2006). Hence, the FSR significantly shows the performance of the microring. Many efforts have been made to enhance the FSR, such as a double Vernier Panda-ring resonator with the maximum FSR of 90 nm (Seyfari et al., 2021), a microring with multi-Mach–Zehnder interferometers with FSR over 88 nm (Y. Chen & Qiu, 2021), a compact microring resonator using low-loss bends with FSR of 35 nm (Song et al., 2020), and a racetrack microring resonator with Fabry–Perot cavities where the FSR is over 150 nm (Kumar Bag & Varshney, 2021).

By integrating Fano resonance with the microring resonance, the FSR can be improved. The Fano resonance was applied in the microring technology through many methods such as photonic crystal cavity generation (Peng et al., 2018), nanocavities utilization in split-ring resonator (Zhang et al., 2013), double half ring resonator (He et al., 2021), and side coupled ring cavity with a metal nanowall (F. Chen et al., 2019). Fano resonance can be obtained through the interference of a continuous background mode and a discrete resonant mode (Li & Bogaerts, 2017; Zhao et al., 2016). The main attribute of Fano resonance is the asymmetric line shape which is caused by the two-resonance optical

Received: June 20, 2022
Accepted: August 8, 2022
Published: October 31, 2023

DOI: https//doi.org/10.22452/mjs.vol42no3.3
Malaysian Journal of Science 42(3): 13-19 (October 2023)

interference (Zhao et al., 2016). In this case, the Fano resonance is achieved by merging the circulation resonance from the ring with the Fabry–Perot resonance from the bus waveguide (Yi et al., 2010). Fano resonance also offers the potential to enhance the performance of the microring in terms of FSR, LOD, and sensitivity (Chao & Guo, 2003; Tu et al., 2017; Wang et al., 2017). However, the generated Fabry–Perot resonance, which is essential to produce the Fano resonance, has a small FSR that will affect the overall spectrum (Yi et al., 2010).

In this work, an optimized racetrack microring resonator configuration was proposed to reduce the effect of Fabry–Perot resonance, thus enhancing the FSR. Since the configuration involves a racetrack microring resonator and Fano resonance, the system is called integrated Fano-racetrack microring (IFM) configuration. For this research, two simulations were performed to achieve the maximum FSR: 1) Comparison of the resonance between IFM and conventional racetrack configuration and 2) the optimization process of IFM configuration. The optimization was performed to determine the maximum FSR with various configuration parameters such as ring radius, length of the racetrack, and distance of the reflectors from the center.

2. Model and Theory

The simulation was performed for two types of racetrack microring resonators: (1) the conventional racetrack microring resonator and (2) the racetrack microring resonator with reflectors in the bus waveguide. Figure 1 a) and b) shows both configurations with the labelled propagated electric field. The figure shows that only the IFM configuration was installed with reflectors in the bus waveguide. The reflectors play a major role in the IFM configuration to generate the Fano resonance.

Light is travelled through the input port, E_{in} and propagated in the waveguide. At the coupling region, a fraction of the light is coupled into the ring at E_1, and another fraction is still propagating in the waveguide. The propagating light in the waveguide is partially reflected due to the presence of the reflector and partially went through the output port, E_{out}. On the other hand, light in the ring is propagated towards the coupling region at E_2 and coupled back into the waveguide. Then, the resonance from the ring is merged with the resonance in the waveguide, thus Fano-like resonance is obtained. It is necessary for the bus reflector to be made of partial reflective materials to generate the Fabry–Perot resonance (Yi et al., 2010). The combination of circulation resonance and Fabry–Perot resonance can create a Fano resonance as the output spectrum.

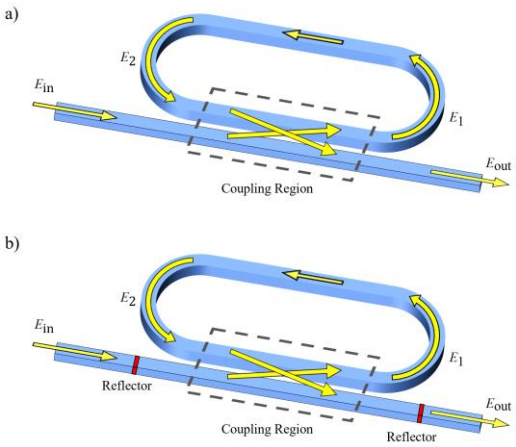

Figure 1. a) The conventional and b) the IFM configuration racetrack configurations.

The mathematical theory of optical coupling was performed for the IFM configuration to construct the numerical programming script. The coupling theory and optical phase shift with the attenuation loss were included in the computation. The transfer matrix for the whole integration system comprises the microring and Fabry–Perot resonances (Gu et al., 2019) can be expressed as follows:

$$\begin{bmatrix} E_{out} \\ E_1 \end{bmatrix} = \frac{1}{i\sqrt{1-r_h^2}} \begin{bmatrix} -1 & -r_h \\ r_h & 1 \end{bmatrix} \cdot \begin{bmatrix} e^{i2\pi n_{eff} L/\lambda} & 0 \\ 0 & e^{-i2\pi n_{eff} L/\lambda} \end{bmatrix} \cdot \begin{bmatrix} t_R & 0 \\ 0 & 1 \end{bmatrix} \cdot \begin{bmatrix} e^{i2\pi n_{eff} L/\lambda} & 0 \\ 0 & e^{-i2\pi n_{eff} L/\lambda} \end{bmatrix} \cdot \frac{1}{i\sqrt{1-r_h^2}} \begin{bmatrix} -1 & -r_h \\ r_h & 1 \end{bmatrix} \cdot \begin{bmatrix} E_{in} \\ E_2 \end{bmatrix} \quad (1)$$

where E_{in} is the input port, E_{out} is the output port, E_1 is the input port to the ring, and E_2 is the output port of the ring. The term n_{eff} is the effective refractive index, which represents both refractive indexes of core and cladding. L represents the distance between the reflector in the waveguide and t_R is the optical transfer function (OTF) of the racetrack microring resonator. The amplitude reflection coefficient (Yi et al., 2010) can be expressed as follows:

$$r_h = \frac{n_{eff}-1}{1-n_{eff}}. \quad (2)$$

DOI: https//doi.org/10.22452/mjs.vol42no3.3
Malaysian Journal of Science 42(3): 13-19 (October 2023)

The OTF of racetrack microring (Bogaerts et al., 2012; Heebner et al., 2008) is given as below:

$$\frac{E_{out}}{E_{in}} = \frac{c - ae^{i2\pi nL_R/\lambda}}{1 - ca e^{i2\pi nL_R/\lambda}} \quad (3)$$

where a is the single-pass amplitude and expressed as follows (Bogaerts et al., 2012; Heebner et al., 2008; Noorden et al., 2020):

$$a = \exp(-\alpha L_R) \quad (4)$$

where α is the attenuation coefficient and L_R is the perimeter of the all-pass microring resonator. c is a self-coupling coefficient which can be expressed as follows (Noorden et al., 2020):

$$c = \sqrt{1-\kappa}\sqrt{1-\gamma} \quad (5)$$

where κ is the coupling coefficient (Noorden et al., 2020) and γ is the propagation loss coefficient (Noorden et al., 2020).

In this study, the numerical simulation was conducted using a mathematical computation software named Gnu Octave. The Gnu Octave has a high capability in solving numerical computations and presenting data due to its powerful visualisation tools (GNU Octave, n.d.) The simulated configurations are racetrack microring with reflectors embedded in the waveguide and conventional racetrack microring. The core and substrate materials are silicon (Si) and silicon oxide (SiO_2), respectively. The cladding of the microring is air. Due to the difference in refractive index among the materials, resonance confinement can be achieved. The coupling coefficient was set as constant throughout the research.

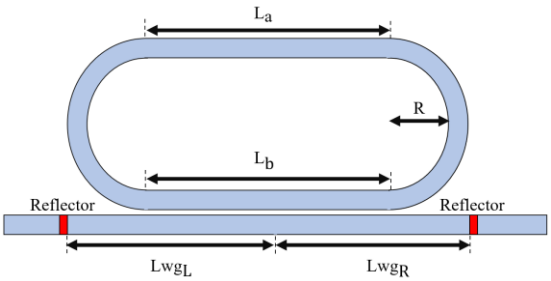

Figure 2. The optimised parameters of the configuration.

The reflectors labelled in Figure 2 are necessary to generate the Fano resonance. The reflector aids in creating interference through Fabry–Perot resonance in the waveguide (Yi et al., 2010). From Figure 2, the perimeter of the system can be calculated as follows:

$$L_R = 2\pi R + L_a + L_b \, . \quad (4)$$

where L_a and L_b are the length of the racetrack microring. Lwg_L and Lwg_R represent the distance of the reflector from the centre of the waveguide.

Table 1. The range of optimisation for all the parameters based on two configurations.

Parameter	Integrated Fano-Microring	Conventional Microring
R	2 μm – 20 μm	2 μm – 20 μm
L_a	10 μm – 30 μm	10 μm – 30 μm
L_b	10 μm – 30 μm	10 μm – 30 μm
Lwg_L	2 μm – 20 μm	-
Lwg_R	2 μm – 20 μm	-

The optimisation of both configurations was performed based on the exhaustive search technique, where each configuration was initialised by considering all parameters' domain as shown in Table 1. For each range of the parameter, 20 values were iterated to observe the FSR. The FSR for each configuration was measured accordingly to analyse the Fano resonance. Both conventional and IFM configurations with the highest FSR were analysed and discussed in the next section. Note that since conventional microring does not have the reflector in the waveguide, only the radius and length of the racetrack were considered.

DOI: https//doi.org/10.22452/mjs.vol42no3.3
Malaysian Journal of Science 42(3): 13-19 (October 2023)

3. Results and Discussions

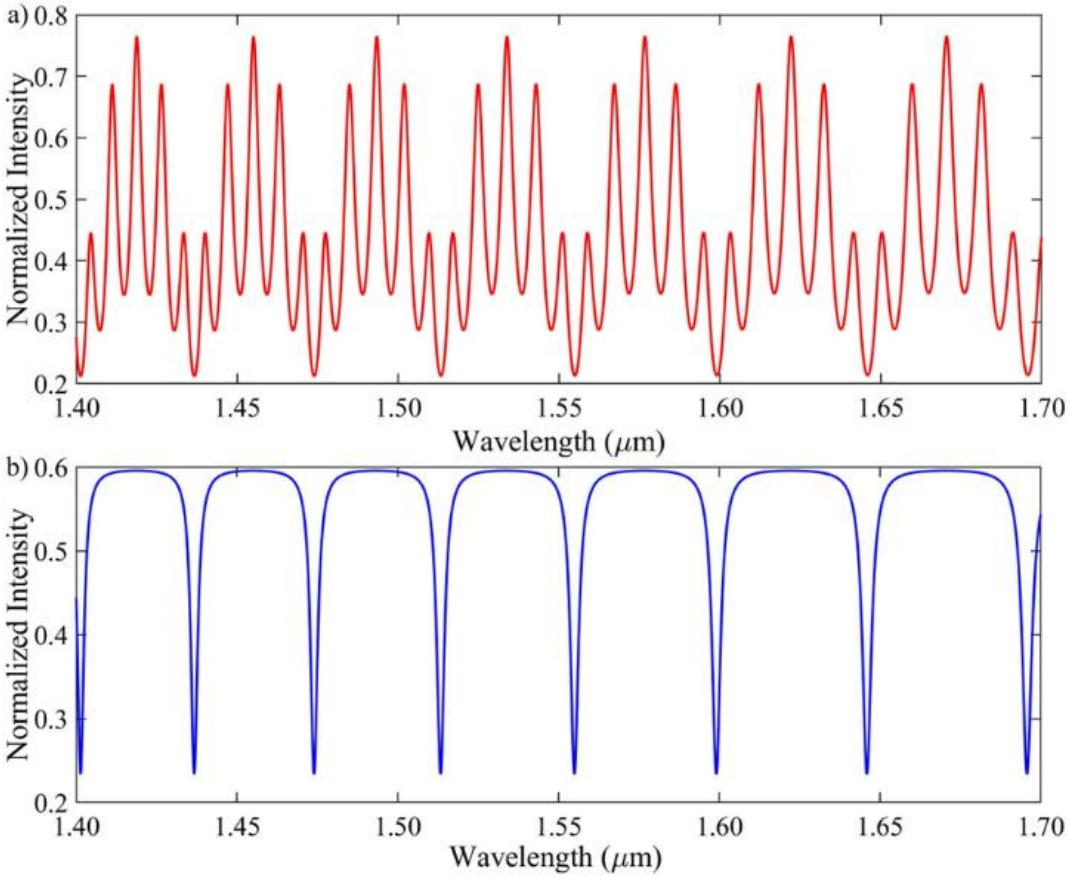

Figure 3. Output numerical simulation of a) IFM spectrum and b) conventional microring spectrum.

Figure 3 depicts the spectrum of IFM comprises numerous peaks compared to the conventional microring. Note that the position of the Lorentzian shape is similar between the two. Besides, the IFM configuration also exhibits a characteristic of Vernier effect where the resonance pattern becomes enveloped in a group (Gomes et al., 2021). The IFM spectrum also shows a Fano-like line shape credited to the reflectors in the waveguide where a fraction of the resonance still propagates in the waveguide causing the interference of numerous resonances with different phase shifts (Yi et al., 2010). The conventional microring spectrum differs from the IFM spectrum due to the suppression of interstitial peak by Fano resonance (Boeck et al., 2010).

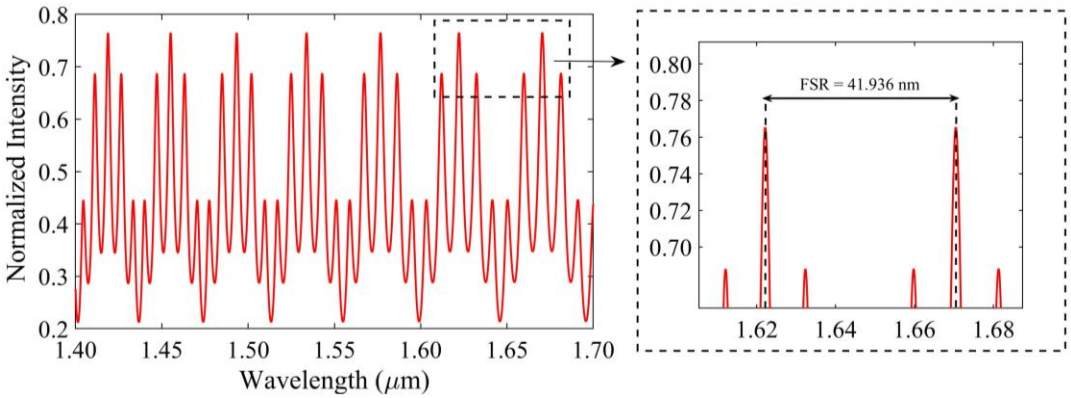

Figure 4. The unoptimised IFM spectrum and the magnified peaks for FSR measurement.

Figure 4 shows the unoptimised spectrum of IFM and the recorded FSR was 41.936 nm. Without optimising the simulation system, the IFM spectrum has a very low FSR, which will reduce the performance of the microring. This is because, the Fabry–Perot resonance with small FSR merges with the circulation resonance (Yi et al., 2010). The collective small FSR from the

DOI: https//doi.org/10.22452/mjs.vol42no3.3
Malaysian Journal of Science 42(3): 13-19 (October 2023)

Fabry–Perot resonance affects the microring spectrum by suppressing its peaks and producing a lot of smaller peaks. Subsequently, the FSR, instead of increasing, decreases tremendously. Therefore, the optimisation process is essential to improve the performance of the microring.

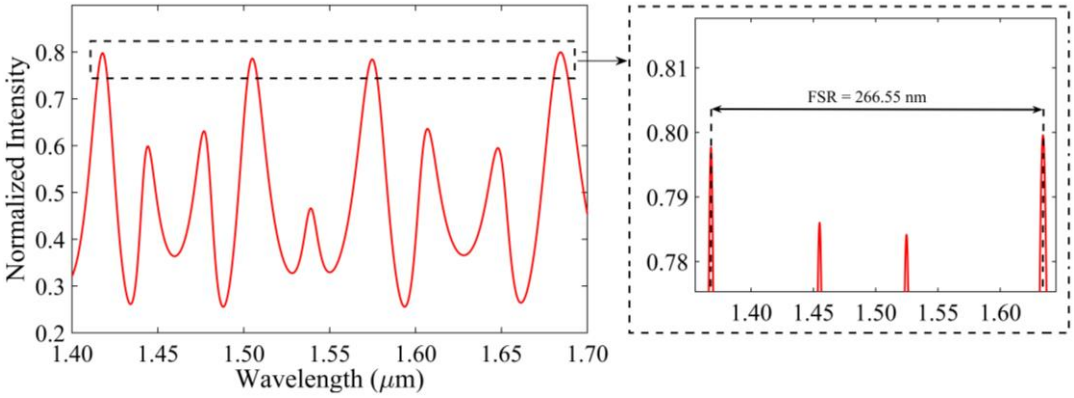

Figure 5. The optimised IFM and the magnified peaks for FSR measurement.

Figure 5 illustrates the optimised IFM spectrum where the measured FSR was 266.55 nm. The FSR of the optimised configuration was five times higher than that of the unoptimised configuration. The parameters of the optimised IFM configuration are tabulated in Table 2.

Table 2. The optimized IFM configuration

Parameter	Value
R	15.26 μm
L_a	30.00 μm
L_b	30.00 μm
Lwg_L	2.95 μm
Lwg_R	2.00 μm

The main contributor to the wide FSR of the IFM configuration is the Fano resonance which suppresses the interstitial resonances (Boeck et al., 2010; Schwelb, 2007). Due to the suppression of interstitial peaks in the spectrum, the Vernier effect can be observed, and the Vernier effect helps to extend the FSR of the resonance (Jin et al., 2011; Troia et al., 2014). This is because, the waveguide system of IFM consists of two resonances type: (1) circulation resonance from racetrack waveguide and (2) Fabry–Perot resonance from the reflector at the bus waveguide. In the sensing application, a large FSR benefits the system because it contributes to wider measurement range (C. Chen et al., 2021; Tian et al., 2020). Besides, wide FSR helps the system to distinguish the resonance peak and makes the detection system more accurate especially in all-optical sensing technologies. Even though the FSR is detrimental to the quality factor (QF) (Taufiqurrahman et al., 2020), high FSR is beneficial to achieve high optical sensitivity because the QF does not impose a direct impact on the sensing application. Nevertheless, the simulated system has successfully optimised the FSR of the system based on the IFM waveguide with the reflectors.

4. Conclusion

In conclusion, two simulations were performed to convey the significance of Fano resonance in the application of microring technology. The first simulation indicates the difference between the conventional racetrack microring resonator with the IFM resonator. With the suppression by the Fano resonance, the vernier effect can be achieved, hence the FSR can be increased significantly. In the second simulation, the system was optimized successfully and a comparison between the unoptimized and optimized Fano resonance was made. The FSR of the optimized Fano resonance was 266.55 nm, which is five times higher that of the unoptimized. These simulations prove that the IFM spectrum has a huge potential and much room to be improved. Furthermore, the Fano resonance will likely help to improve the sensitivity due to its profile having numerous sharp peaks (Zhao et al., 2016). The sharp peaks may be vital in getting a more significant wavelength shift; hence, the sensitivity of the microring increase.

5. Acknowledgement

This work was supported by CAPTOR and the Department of Physics, International Islamic University Malaysia in term of facilities and financially by the Ministry of Education (Malaysia) through Fundamental Research Grant Scheme (Project No.: FRGS 19-033-0641) (References No.: FRGS/1/2018/TK07/UIAM/02/1).

6. References

Bavili, N., Balkan, T., Morova, B., Eryürek, M., Uysallı, Y., Kaya, S., & Kiraz, A. (2020). Highly sensitive optical sensor for hydrogen gas based on a polymer microcylinder ring resonator. *Sensors and Actuators B: Chemical*, *310*, 127806.

Bharti, G. K., & Rakshit, J. K. (2021). Design of all-optical logical mode-switching using micro-ring resonator. *Optical Engineering*, *60*(3), 035103.

Biswas, U., Rakshit, J. K., Das, J., Bharti, G. K., Suthar, B., Amphawan, A., & Najjar, M. (2021). Design of an ultra-

DOI: https//doi.org/10.22452/mjs.vol42no3.3
Malaysian Journal of Science 42(3): 13-19 (October 2023)

compact and highly-sensitive temperature sensor using photonic crystal based single micro-ring resonator and cascaded micro-ring resonator. *Silicon*, *13*(3), 885–892.

Boeck, R., Jaeger, N. A. F., & Chrostowski, L. (2010). Experimental demonstration of the Vernier effect using series-coupled racetrack resonators. *2010 International Conference on Optical MEMS and Nanophotonics*, 1–2.

Bogaerts, W., de Heyn, P., van Vaerenbergh, T., de Vos, K., Kumar Selvaraja, S., Claes, T., Dumon, P., Bienstman, P., van Thourhout, D., & Baets, R. (2012). Silicon microring resonators. *Laser & Photonics Reviews*, *6*(1), 47–73.

Chao, C. Y., & Guo, L. J. (2003). Biochemical sensors based on polymer microrings with sharp asymmetrical resonance. *Applied Physics Letters*, *83*(8). https://doi.org/10.1063/1.1605261

Chao, C. Y., & Guo, L. J. (2006). Design and optimization of microring resonators in biochemical sensing applications. *Journal of Lightwave Technology*, *24*(3), 1395–1402. https://doi.org/10.1109/JLT.2005.863333

Chen, C., Hou, X., & Wang, J. (2021). A Novel Hybrid Plasmonic Resonator with High Quality Factor and Large Free Spectral Range. *IEEE Sensors Journal*, *21*(2). https://doi.org/10.1109/JSEN.2020.3017647

Chen, F., Zhang, H., Sun, L., Li, J., & Yu, C. (2019). Temperature tunable Fano resonance based on ring resonator side coupled with a MIM waveguide. *Optics & Laser Technology*, *116*, 293–299.

Chen, Y., & Qiu, Q. (2021). A novel microring resonator based on multi-Mach–Zehnder interferometers. *Optics Communications*, *483*. https://doi.org/10.1016/j.optcom.2020.126643

GNU Octave. (n.d.). Retrieved July 14, 2022, from https://octave.org/

Gomes, A. D., Bartelt, H., & Frazão, O. (2021). Optical Vernier Effect: Recent Advances and Developments. In *Laser and Photonics Reviews* (Vol. 15, Issue 7). https://doi.org/10.1002/lpor.202000588

Gu, L., Fang, H., Li, J., Fang, L., Chua, S. J., Zhao, J., & Gan, X. (2019). A compact structure for realizing Lorentzian, Fano, and electromagnetically induced transparency resonance lineshapes in a microring resonator. *Nanophotonics*, *8*(5), 841–848.

Guider, R., Gandolfi, D., Chalyan, T., Pasquardini, L., Samusenko, A., Pederzolli, C., Pucker, G., & Pavesi, L. (2015). Sensitivity and limit of detection of biosensors based on ring resonators. *Sensing and Bio-Sensing Research*, *6*, 99–102.

He, Q., Huo, Y., Guo, Y., Niu, Q., Hao, X., Cui, P., Wang, Y., & Song, M. (2021). Multiple adjustable Fano resonance based on double half ring resonator and its application. *Physica Scripta*, *96*(6), 065504.

Heebner, J., Grover, R., & Ibrahim, T. (2008). *Optical microresonator theory*. Springer.

Jin, L., Li, M., & He, J. J. (2011). Highly-sensitive silicon-on-insulator sensor based on two cascaded micro-ring resonators with vernier effect. *Optics Communications*, *284*(1). https://doi.org/10.1016/j.optcom.2010.08.035

Kim, K. W., Song, J., Kee, J. S., Liu, Q., Lo, G.-Q., & Park, M. K. (2013). Label-free biosensor based on an electrical tracing-assisted silicon microring resonator with a low-cost broadband source. *Biosensors and Bioelectronics*, *46*, 15–21.

Koushik, K. P., & Malathi, S. (2020). Optical micro-ring resonator for detection of carbon dioxide gas. In *Emerging Trends in Photonics, Signal Processing and Communication Engineering* (pp. 157–161). Springer.

Kumar Bag, S., & Varshney, S. K. (2021). Ultrawide FSR microring racetrack resonator with an integrated Fabry–Perot cavity for refractive index sensing. *Journal of the Optical Society of America B*, *38*(5). https://doi.org/10.1364/josab.416454

Li, A., & Bogaerts, W. (2017). An actively controlled silicon ring resonator with a fully tunable Fano resonance. *APL Photonics*, *2*(9), 096101.

Moradi, M., Mohammadi, M., Olyaee, S., & Seifouri, M. (2021). Design and simulation of a fast all-optical modulator based on photonic crystal using ring resonators. *Silicon*, 1–7.

Noorden, A. F. A., Mohamad, A., Salleh, M. H., Daud, S., Mohamad, S. N., & Ali, J. (2020). Free spectral range analysis of double series microresonator system for all-optical corrosion sensor. *Optical Engineering*, *59*(1), 17106.

Peng, F., Wang, Z., Yuan, G., Guan, L., & Peng, Z. (2018). High-sensitivity refractive index sensing based on Fano resonances in a photonic crystal cavity-coupled microring resonator. *IEEE Photonics Journal*, *10*(2), 1–8.

Schwelb, O. (2007). The nature of spurious mode suppression in extended FSR microring multiplexers. *Optics Communications*, *271*(2). https://doi.org/10.1016/j.optcom.2006.10.053

DOI: https//doi.org/10.22452/mjs.vol42no3.3
Malaysian Journal of Science 42(3): 13-19 (October 2023)

Seyfari, A. K., Bahadoran, M., & Aghili, A. (2020). Ultra-sensitive pressure sensor using double stage racetrack silicon micro resonator. *Optical and Quantum Electronics*, *52*(9), 1–16.

Seyfari, A. K., Bahadoran, M., & Yupapin, P. (2021). Design and modeling of double Panda-microring resonator as multi-band optical filter. *Nano Communication Networks*, *29*. https://doi.org/10.1016/j.nancom.2021.100352

Singh, M. P., Hossain, M., Rakshit, J. K., Bharti, G. K., & Roy, J. N. (2021). Proposal for polarization rotation–based ultrafast all optical switch in ring resonator. *Brazilian Journal of Physics*, *51*(6), 1763–1774.

Song, J. H., Kongnyuy, T. D., de Heyn, P., Lardenois, S., Jansen, R., & Rottenberg, X. (2020). Compact Micro-Ring Resonator using Low-Loss Silicon Waveguide Bends. *Conference Proceedings - Lasers and Electro-Optics Society Annual Meeting-LEOS*, *2020-May*.

Taufiqurrahman, S., Dicky, G., Estu, T. T., Daud, P., Mahmudin, D., & Anshori, I. (2020). Free spectral range and quality factor enhancement of multi-path optical ring resonator for sensor application. *AIP Conference Proceedings*, *2256*. https://doi.org/10.1063/5.0014960

Tian, C., Zhang, H., Li, W., Huang, X., Liu, J., Huang, A., & Xiao, Z. (2020). Temperature sensor of high-sensitivity based on nested ring resonator by Vernier effect. *Optik*, *204*, 164118.

Troia, B., Khokhar, A. Z., Nedeljkovic, M., Penades, J. S., Passaro, V. M. N., & Mashanovich, G. Z. (2014). Cascade-coupled racetrack resonators based on the Vernier effect in the mid-infrared. *Optics Express*, *22*(20), 23990–24003.

Tu, Z., Gao, D., Zhang, M., & Zhang, D. (2017). High-sensitivity complex refractive index sensing based on Fano resonance in the subwavelength grating waveguide micro-ring resonator. *Optics Express*, *25*(17). https://doi.org/10.1364/oe.25.020911

Vollmer, F., & Schwefel, H. G. L. (2014). Taking detection to the limit with optical microcavities: Recent advances presented at the 560. WE Heraeus Seminar. In *The European Physical Journal Special Topics* (Vol. 223, Issue 10, pp. 1907–1916). Springer.

Wang, G., Dai, T., Jiang, J., Yu, H., Hao, Y., Wang, Y., Li, Y., Jiang, X., & Yang, J. (2017). Slope tunable Fano resonances in asymmetric embedded microring resonators. *Journal of Optics (United Kingdom)*, *19*(2). https://doi.org/10.1088/2040-8986/aa51a1

Yi, H., Citrin, D. S., & Zhou, Z. (2010). Highly sensitive silicon microring sensor with sharp asymmetrical resonance. *Optics Express*, *18*(3), 2967–2972.

Zhang, Q., Wen, X., Li, G., Ruan, Q., Wang, J., & Xiong, Q. (2013). Multiple magnetic mode-based Fano resonance in split-ring resonator/disk nanocavities. *Acs Nano*, *7*(12), 11071–11078.

Zhao, G., Zhao, T., Xiao, H., Liu, Z., Liu, G., Yang, J., Ren, Z., Bai, J., & Tian, Y. (2016). Tunable Fano resonances based on microring resonator with feedback coupled waveguide. *Optics Express*, *24*(18), 20187–20195.

Zhu, J., & Lou, J. (2020). High-sensitivity Fano resonance temperature sensor in MIM waveguides coupled with a polydimethylsiloxane-sealed semi-square ring resonator. *Results in Physics*, *18*, 103183.

DOI: https//doi.org/10.22452/mjs.vol42no3.3
Malaysian Journal of Science 42(3): 13-19 (October 2023)